Automatic Detection of Ostia in the Left Atrium

Matthias Hoffmann[1], Martin Koch[1], Norbert Strobel[2], Andreas Maier[1,3]

[1]Pattern Recognition Lab, Friedrich-Alexander-Universität Erlangen-Nürnberg, Erlangen, Germany
[2]Siemens Healthcare GmbH, Forchheim, Germany
[3]Erlangen Graduate School in Advanced Optical Technologies (SAOT), Erlangen, Germany
matthias.hoffmann@cs.fau.de

Abstract. Atrial fibrillation is a wide spread heart arrhythmia that can be treated by catheter ablation. This procedure may involve a planning step which can be performed based on a 3-D model of the patient's left atrium (LA) segmented from a CT or MRI volume. One of the first decisions to make during treatment is whether to use a single-shot device or a radio-frequency catheter. This decision is based on the size of pulmonary vein ostium and the ablation path as defined by ablation lines. Recently a method for automatic annotation of ablation lines was proposed. It is based on the position of the pulmonary (PV) vein ostia of a left atrium. To facilitate a fully automatic approach, we present a novel learning-based method based on mesh skeletonization that automatically detects pulmonary vein ostium positions in a 3-D LA model. In our evaluation, we found a success rate of 86 % and an average error of 4.3±2.6 mm.

1 Introduction

Cardiac ablation is a common treatment option for atrial fibrillation (AFib). It is performed minimally invasively [1] using catheters. During an ablation that follows the wide-area circumferential ablation approach, transmural lesions are created along a path around both left pulmonary veins and both right pulmonary veins, respectively. These lesions can, for example, be created by taking a cryo-balloon device which is pushed into the pulmonary vein (PV) ostia. By cooling the balloon with liquid nitrogen, surrounding tissue is destroyed and ring-shaped lesions are created. The selection of a balloon diameter that matches the anatomy is important for the long-term outcome of the procedure. This selection is performed based on a 3-D model of the left atrium which was segmented from a CT or MRI scan of the patient. A software tool can be used to help the physician with the decision [2]. An automatic localization of pulmonary vein ostia could make this process more user-friendly or even automatize the decision process.

Another option is ablation by tissue heating. This can be performed using a radio-frequency (RF) catheter. This catheter is able to create point-shaped lesions to form, point-by-point, a path of overlapping, consecutive lesions around the PV ostia. Guidance during RF ablation procedures is often done using an

electro-anatomical mapping system. Here, the 3-D position of the catheter is determined using, e.g., the electrical impedance. This allows to render catheters in the context of a 3-D model of the patient's left atrium (LA). An alternative navigation method is augmented fluoroscopy [3]. Here the 3-D model is registered to fluoroscopic images and overlaid on them. In both cases, lines representing the planned ablation regions can be displayed on the 3-D model to facilitate orientation during the procedure. Recently, an approach for automatic transfer of ablation lines from a reference model annotated with reference ablation lines was proposed [4]. This approach, as well as an approach for selection of C-arm viewing angles [5], require the position of the PV ostia as input. Previously, this was obtained by manual annotation.

Recent segmentation approaches were designed such that the pulmonary veins are treated separately from the atrial body [6,7]. Karim et al. [6] proposed a three-step approach in which first, the complete left atrium is segmented using a manually placed seed point and an interactive bounding box. Then, within the LA, the atrial body is segmented and finally, based on a vesselness score, pulmonary vein centerlines are extracted and tracked to, e.g. measure the diameter interactively. Zheng et al. [7] use a model-based approach to segment the left atrial body, four PVs and the left atrial appendage (LAA). These parts are later merged together. However, the main focus of both approaches is the overall segmentation accuracy of atrium and PV trunks but not on the precise location of the PV ostia. Rettmann et al. [8] presented a semi-automatic approach for PV ostium localization on a segmented volume. This method requires the user to manually click on each of the four pulmonary veins to compute a centerline. For each centerline point, the crossection area of the PV is calculated and the first point where the crossection area increases significantly is considered as ostium.

We present a method designed for an explicit localization of PV ostia in a LA which is available as a triangle mesh. Since our approach works on a model, it is independent of the modality and the segmentation tool.

2 Materials and Methods

Our approach is a learning based method that relies on features of a skeletonization of the LA triangle mesh $\mathcal{M} = (\mathcal{V}_\mathcal{M}, \mathcal{E}_\mathcal{M})$ consisting of vertices $\mathcal{V}_\mathcal{M}$ and edges $\mathcal{E}_\mathcal{M}$. We describe first, how the skeleton is generated and describe then the features used for classification of PV ostia.

2.1 Mesh skeletonization

As we seek for a skeletonization not only of each tubular PV as in [6] but of the whole LA, a more complicated skeletonization approach is required. We decided for the method by Telea et al. [9] which comprises two steps: First, a so-called surface skeleton is computed. This is a 2-D manifold consisting of all points which are center of spheres inscribed by the mesh. Then, the mesh-property is restored and a gradient field is implicitly defined on the surface skeleton. The

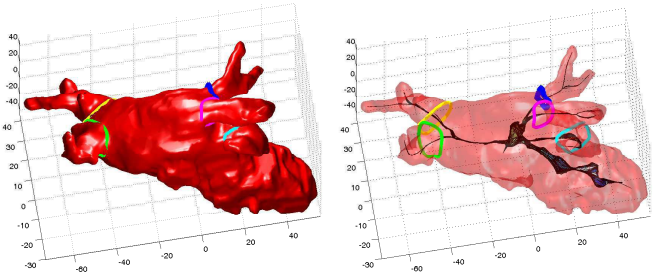

(a) (b)

Fig. 1. (a) LA with annotated ostia and left atrial appendage (cyan). (b) The curve skeleton is obtained by moving iteratively points of the surface skeleton along an implicitly defined vector field.

surface skeleton points are now moved iteratively along this gradient field until they converge along the singularities of the gradient field which form the so-called curve skeleton. The result of this method is a shrunken mesh $\mathcal{C} = (\mathcal{V}_\mathcal{C}, \mathcal{E}_\mathcal{C})$ along the curve-skeleton, see Figure 1(b)

Our goal is to model the curve skeleton explicitly by a small number of cubic splines. We therefore seek for a subset of points and edges of this curve-skeleton mesh that defines an abstract graph structure which allows to extract the main lines along this mesh. To this end, a shortest path tree on $\mathcal{C}$ is computed. The root of the tree is defined to be the point $\boldsymbol{r} \in \mathbb{R}^3$ of the points in $V_\mathcal{C}$ that is closest to the distance to the center of gravity of the points of the original mesh $\mathcal{M}$, i.e.

$$\boldsymbol{r} = \arg\min_{\boldsymbol{p} \in \mathcal{V}_\mathcal{C}} \left|\left| \boldsymbol{p} - \tfrac{1}{|\mathcal{V}_\mathcal{M}|} \textstyle\sum_{\boldsymbol{p}' \in \mathcal{V}_\mathcal{M}} \boldsymbol{p}' \right|\right|_2 . \tag{1}$$

We then select from the shortest path tree the main branches. This is performed in an iterative way by creating a new tree to which successively new branches are added. In each iteration, the longest branch of the shortest path tree is selected and added to the new tree as a first step. Then, all branches in the shortest path tree, that have a leaf node which is close to the selected branch are removed. This is repeated until the shortest path tree is empty.

After removing very short branches, each path from a leave to the root is transformed into a cubic spline curve. The curve is defined as $\mathcal{S}(t) \rightarrow \boldsymbol{x} \in \mathbb{R}^3$ where t is the distance along the spline to the center $\boldsymbol{r}$ of the left atrium and $\boldsymbol{x}$ defines the 3-D coordinate with respect to the LA center of gravity which is the origin of the coordinate system.

2.2 Feature Computation

The most important feature that we use is the radius $r(\mathcal{S}(t))$ of the pulmonary vein at a 3-D position $\mathcal{S}(t)$. As the PV crossection may be more elliptical than circular, we first compute the crossection plane defined by the point $\mathcal{S}(t)$ and the normal vector $\nabla\mathcal{S}(t)$. Then we compute the intersection of the PV with this

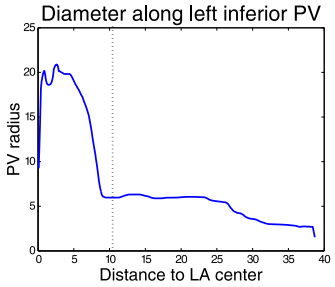

Fig. 2. Diameter of the pulmonary vein with respect to the distance to the LA center. The dotted line indicates the position of the PV ostium.

Table 1. Features used for ostium classification

Feature for point $\mathcal{S}(t)$	Description
$r(\mathcal{S}(t')), t' \in \{t-7 \dots t+1\}$	Radius at position $\mathcal{S}(t)$ and its vicinity
$\frac{\mathrm{d}r(\mathcal{S}(t'))}{\mathrm{d}t'}, t' \in \{t-7 \dots t+1\}$	Diameter increase at position $\mathcal{S}(t)$ and its vicinity
$\max_{t'>t} r(\mathcal{S}(t'))$	maximum radius in distal direction
$\min_{t'<t} r(\mathcal{S}(t'))$	minimum radius in proximal direction
$\mathcal{S}(t)$	3-D position
$\nabla\mathcal{S}(t)$	direction of PV
t	distance to the LA center

plane and select the median distance from $\mathcal{S}(t)$ to the PV points yielded by the intersection. Afterwards, a spatial median filtering is applied to the radii along the PV. The PV ostium is characterized by an increase of the diameter towards the LA center, see Figure 2. Therefore, we use not only the radius at t as a feature to classify whether a ostium is at position $\mathcal{S}(t)$, but also the radii

$$r(\mathcal{S}(t')), t' \in \{t-7 \dots t+1\} \tag{2}$$

in the neighborhood. To capture the increase of the diameter, also the derivatives of the diameter in the vicinity of are used as features.

To make sure that the large increase at position $r(\mathcal{S}(t))$ is not due to a local minimum of the PV diameter, we add the maximum radius in distal direction as feature. To distinguish the PV ostium from a local widening, e.g., caused by merging of two smaller veins, the minimum radius is also considered as feature. Additional features are described in Tab. 1 which gives an overview of all features.

2.3 Classification and Ostium Detection

For each point along the splines representing the branches of the curve skeleton, the set of features is computed. A decision tree is used to classify the set $\mathcal{O}$ of points that belong to an ostium. In a second stage, this group is split up to points $\mathcal{O}_{\text{left}}$ belonging to a left PV ostium and points $\mathcal{O}_{\text{right}}$ of right PV ostia using, again, a trained classifier. Clustering of the points is performed based on a connected components approach considering all points with a distance below

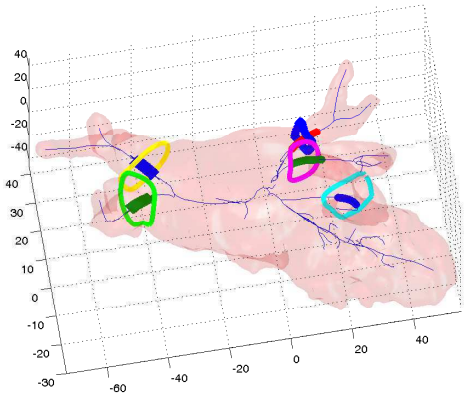

Fig. 3. LA skeleton (blue lines) with positions classified as belonging to a PV ostium. These positions are colored according to the clustering result. Additionally, the ground truth annotations of LAA (cyan circle) and PV ostia (other circles) are shown.

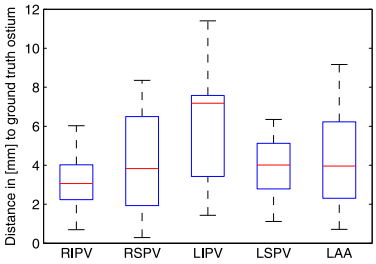

Fig. 4. Detection results grouped for right inferior and superior vein (RIPV and RSPV, respectively), left inferior and superior vein (LIPV and LSPV, respectively), and the left atrial appendage (LAA).

a threshold as connected. An example of this clustering is shown in Figure 3. Then, the largest cluster on the right side is considered as first right PV. All points in $\mathcal{O}_{\text{right}}$ that are behind this cluster are removed from $\mathcal{O}_{\text{right}}$. Then the remaining largest cluster is considered as the other right PV. This procedure is performed for the left side similarly. However, here are three clusters extracted to also find the place where the left atrial appendage (LAA) joins the atrium.

3 Experimental Setup and Results

For evaluation, we used nine left atrium meshes from different patients segmented from MRI volumes using InspaceEP (Siemens Healthcare GmbH, Forchheim, Germany). The PV ostia were annotated by a physician, if a LAA was present in the 3-D mesh, it was annotated by an expert. The data comprised in total 36 PV ostia and 8 LAA annotations. Training of the classifier and evaluation was performed as a leave-one-out crossvalidation. We used the MATLAB implementation of the decision tree as classifier. As position error measure, we used the distance of the detected ostium center to the regression plane defined by the ground truth ostium annotation. A detection of a single ostium is counted as not successful if for a PV no cluster was left or if the selected cluster is not located on a PV or the LAA. In our evaluation, we achieved a success rate of 86%. The mean error was 4.3±2.6 mm. The errors for each PV are shown in Figure 4.

4 Discussion

A comparison with the segmentation methods [6,7] is difficult. They report how well the PV was segmented but not the accuracy of the PV ostium localization. Rettman et al. [8] reported a mean error of 1.5 mm 5.0 mm, depending on the PV. These results were slightly better than ours, however, they require user input whereas our method was designed to be fully automatic. Misdetections happened mostly because the LAA was not detected correctly. In one case, the right PVs merged so early that this patient could be considered to have a common ostium. In this case, only one of the two right PVs was detected. The average accuracy is below the 5 mm threshold which is considered as relevant for LA registration [10]. The threshold required for ostium and LAA annotation could be determined by studying the inter-user-variability of physicians. As there is no exact definition of the PV ostium position, it is probably in this range. In any case, the result can serve as initialization for manual annotation that can be, if applicable, refined.

Acknowledgments and Disclaimer. This work was supported by Siemens Healthcare GmbH, Forchheim, Germany. The concepts and information presented in this paper are based on research and are not commercially available.

References

1. Calkins H, Brugada J, Packer DL, et al. HRS/EHRA/ECAS Expert Consensus Statement on Catheter and Surgical Ablation of Atrial Fibrillation. Europace. 2007 June;9(6):335 – 379.
2. Kleinoeder A, Brost A, Bourier F, et al. Cryo-balloon catheter position planning using AFiT. In: Proc. SPIE. vol. 8316; 2012. p. 83162R.
3. Ector J, Buck SD, Huybrechts W, Nuyens D, Dymarkowski S, et al. Biplane three-dimensional augmented fluoroscopy as single navigation tool for ablation of atrial fibrillation: Accuracy and clinical value. Heart Rhythm. 2008 July;5(7):957 – 964.
4. Koch M, Brost A, Bourier F, et al. Automatic planning of atrial fibrillation ablation lines using landmark-constrained nonrigid registration. J Medical Imag. 2014;1(1).
5. Koch M, Hoffmann M, Pfister M, et al. Optimized viewing angles for cardiac electrophysiology ablation procedures. Int J Comput Assist Radiol Surg. 2015;10(5):651–664.
6. Karim R, Mohiaddin R, Rueckert D. Left atrium pulmonary veins: segmentation and quantification for planning atrial fibrillation ablation. In: Proc. SPIE; 2009. p. 72611T–72611T.
7. Zheng Y, John M, Boese J, Comaniciu D. Precise segmentation of the left atrium in C-arm CT volumes with applications to atrial fibrillation ablation. In: Proc IEEE Int Symp Biomed Imaging. IEEE; 2012. p. 1421–1424.
8. Rettmann ME, Holmes III DR, Packer DL, Robb RA. Identification of left pulmonary vein ostia using centerline tracking. In: Proc. SPIE. vol. 7262; 2009. p. 726228–726228–7.
9. Telea A, Jalba AC. Computing Curve Skeletons from Medial Surfaces of 3D Shapes. In: Theory and Practice of Computer Graphics. The Eurographics Assoc.; 2012. .
10. King AP, Boubertakh R, Rhode KS, Ma YL, Chinchapatnam P, Gao G, et al. A subject-specific technique for respiratory motion correction in image-guided cardiac catheterisation procedures. Medical Image Analysis. 2009;13(3):419 – 431.